Microstructure and Mechanical Properties of an Al-Zr-Er High Temperature Alloy Microalloyed with Tungsten

A. R. Farkoosh, David Dunand, and David N. Seidman

Abstract

We studied the possibility of improving the coarsening resistance of nanoprecipitates with the $L1_2$ structure, in an Al-Zr-Er alloy system, by microalloying with slow-diffusing tungsten (W). Dilute Al-Zr-Er-W alloys with and without Si were prepared, cast and isochronally (3 h steps, from 200 to 600 °C) aged to understand the behavior of W and its interactions with Zr and Er in aluminum. The microstructure of these alloys in the as-cast and aged conditions has been studied over relevant length scales in parallel with electrical conductivity and microhardness measurements. In addition to optical microscopy studies, local-electrode atom-probe tomography analyses are performed to investigate the structure of the age-hardening ($L1_2$) nanoprecipitates in selected alloys.

Keywords

Atom-probe tomography • Coarsening resistance • $L1_2$ nanoprecipitates

Introduction

Over the past two decades, Al-based high-temperature alloys, also known as Al superalloys, have been developed utilizing scandium and zirconium as the main alloying elements which form coherent $L1_2$ nanoprecipitates with a core-shell structure (Sc-rich core and Zr-rich shell) upon aging [1–7]. Rare-earth (RE) elements such as erbium and ytterbium are added to further improve the creep resistance [8–14]. These alloys with a high number density (10^{22}–10^{23} m^{-3}) of thermally-stable coherent nanoprecipitates exhibit good creep resistance in the 300–425 °C range (minimum creep rates of $\sim 10^{-8}$ s^{-1} at 300 °C, 50 MPa), outperforming all the commercial aluminum alloys [15, 16]. Recently, attempts have been made to make these alloys economically viable by reducing the Sc content [17, 18] or removing the Sc entirely [19–22] producing more affordable Sc-free alloys based on the Al-Zr-RE system. Wen et al.. [21] have shown that an Al-0.08Zr-0.04Er (in at.%) alloy can achieve a maximum microhardness of ~560 MPa upon aging at 400 °C. The Al_3(Zr,Er) nanoprecipitates formed in this system also exhibit a core-shell structure [21] similar to the Al_3(Sc,Zr) nanoprecipitates in the Al-Sc-Zr system. In this study, we focus on micro-alloying a Sc-free Al-Zr-Er alloy with tungsten, with and without silicon micro-additions, with the purpose of further improving the coarsening resistance of the $L1_2$ nanoprecipitates and mechanical properties. Tungsten is of interest because of its very low diffusivity (5×10^{-23} m^2 s^{-1} at 400 °C) in Al [23]. Despite its low solubility in Al (0.025 at.%) [24], W addition could lead to a lower coarsening rate of the precipitates provided that it partitions strongly to the $L1_2$ phase.

Experimental Procedure

Three alloys (Table 1) were melted in a graphite crucible in an electric resistance furnace using 99.99% pure Al, Al-0.6Zr, Al-1Er, Al-12.2Si, and Al-2W master alloys (all in at.%). The melt was maintained at 900 °C for 2 h, and then cast into a graphite mold preheated at 200 °C and placed on an ice-cooled copper platen prior to casting to enhance directional solidification. The as-cast samples were aged isochronally (3 h steps, from 200 to 600 °C) in air, terminated by water quenching. Vickers microhardness measurements (a minimum of 10 measurements for each sample) were carried out on polished samples using a Duramin-5 microhardness tester (Struers), with a load of 200 g and a

A. R. Farkoosh (✉) · D. Dunand · D. N. Seidman
Department of Materials Science & Engineering, Northwestern University, Evanston, USA
e-mail: farkoosh@northwestern.edu

D. Dunand · D. N. Seidman
Center for Atom-Probe Tomography (NUCAPT), Northwestern University, Evanston, USA

C. Chesonis (ed.), *Light Metals 2019*, The Minerals, Metals & Materials Series,
https://doi.org/10.1007/978-3-030-05864-7_48

Table 1 Chemical composition of the alloys determined by inductively coupled plasma optical emission spectroscopy (ICP-OES)

Alloy	Composition (at.%)					
	Zr	Er	Si	Fe	W	Al
NUZE11	0.110	0.005	<0.01	<0.01	<0.01	Bal.
NUZE11W	0.125	0.005	<0.01	<0.01	0.025	Bal.
NUZE11WS	0.125	0.005	0.1	<0.01	0.024	Bal.

dwell time of 5 s. Electrical conductivity measurements were performed utilizing a Sigmatest 2.069 eddy current instrument (Foerster Instruments, Pittsburgh, PA). For each specimen, five measurements were made at 120, 240, 480, and 960 kHz. Nanotips for three-dimensional (3D) atom-probe tomography (APT) investigations were prepared by a two-step electropolishing technique, details of which are provided in a previous publication [18]. 3-D APT experiments were performed utilizing a laser-pulsed LEAP 5000XS tomograph (Cameca Instruments Inc., Madison, WI) at 30 K in ultrahigh vacuum ($<10^{-8}$ Pa). Picosecond ultraviolet (UV) laser pulses (wavelength = 355 nm) were applied with an energy of 30 pJ per pulse and a pulse repetition rate of 500 kHz while maintaining an average detection rate (number of ions per pulse) of 4%. Data analyses were performed using the program IVAS 3.8.2 (Cameca, Madison, WI) and employing the proximity histogram methodology [25].

Results

Figure 1 displays the as-cast grain microstructure of the Al-0.11Zr-0.005Er, Al-0.125Zr-0.005Er-0.025W and Al-0.125Zr-0.005Er-0.1Si-0.024W alloys which consist of relatively coarse columnar grains (0.7–1 mm). No significant differences in the grain structure of the alloys were observed. Microhardness and electrical conductivity evolution of the alloys during isochronal aging are shown in Fig. 2. Precipitation commences between 375 and 400 °C in the Al-0.11Zr-0.005Er and Al-0.125Zr-0.005Er-0.025W alloys, as evidenced by the increase in the microhardness and the electrical conductivity. The W-modified alloy (Al-0.125Zr-0.005Er-0.025W) behaves similarly to the control alloy (Al-0.11Zr-0.005Er), with a slightly higher peak microhardness (42 MPa at 475 °C). The electrical conductivity of as-cast Al-0.125Zr-0.005Er-0.025W (27.3 ± 0.1 MS m^{-1}) is significantly smaller than Al-0.11Zr-0.005Er (29.6 ± 0.1 MS m^{-1}) because of W additions. In the Si- and W-modified alloy (Al-0.125Zr-0.005Er-0.1Si-0.024W), however, precipitation commences at a lower temperature ($\sim$250 °C) and microhardness increases slowly from 265 ± 4 MPa to 282 ± 6 MPa before a rapid increase at above 325 °C. The first rise in microhardness and conductivity is attributed to the precipitation of Er which is known to be stimulated in the presence of Si; Si–Er dimers are expected to form which are known to diffuse faster than Er [18]. Zr also forms dimers with Si [26] which can diffuse fast enough at low temperatures to assist with the nucleation of the $L1_2$ phase. The peak hardness in this alloy reaches 617 ± 19 MPa which is $\sim$20% higher than that of the Si-free alloys. At higher temperatures, however, hardness declines at nearly the same rate for all three alloys studied, due to coarsening and dissolution of the nanoprecipitates, suggesting that W is not slowing the coarsening kinetics of the $L1_2$ nanoprecipitates.

The Al-0.125Zr-0.005Er-0.1Si-0.024W alloy was studied by APT to determine the composition of the nanoprecipitates in two isochronal aging conditions: 475 °C (peak hardness) and 525 °C (slightly overaged) from Fig. 2a. Figure 3 presents APT reconstructions for these samples. A precipitate number density of 5×10^{22} m^{-3} was measured in the

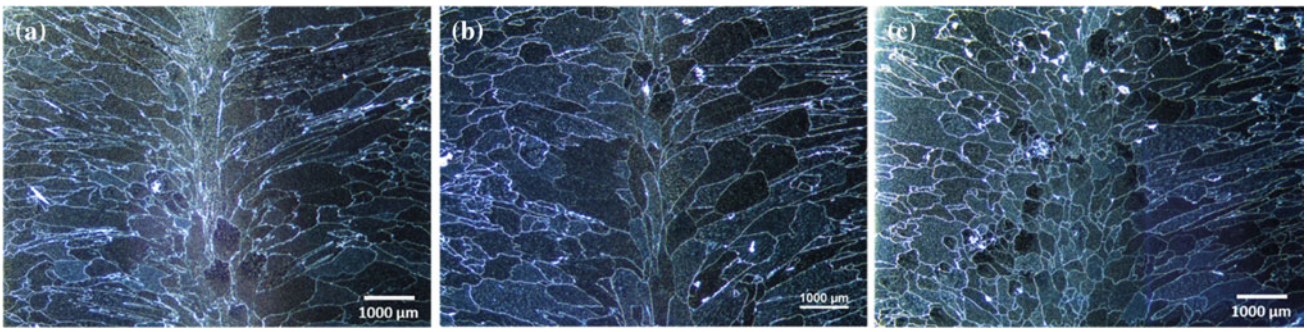

Fig. 1 Optical micrographs of polished, etched (Keller's reagent) cross-sections of as-cast **a** Al-0.11Zr-0.005Er, **b** Al-0.125Zr-0.005Er-0.025 W and **c** Al-0.125Zr-0.005Er-0.1Si-0.024W

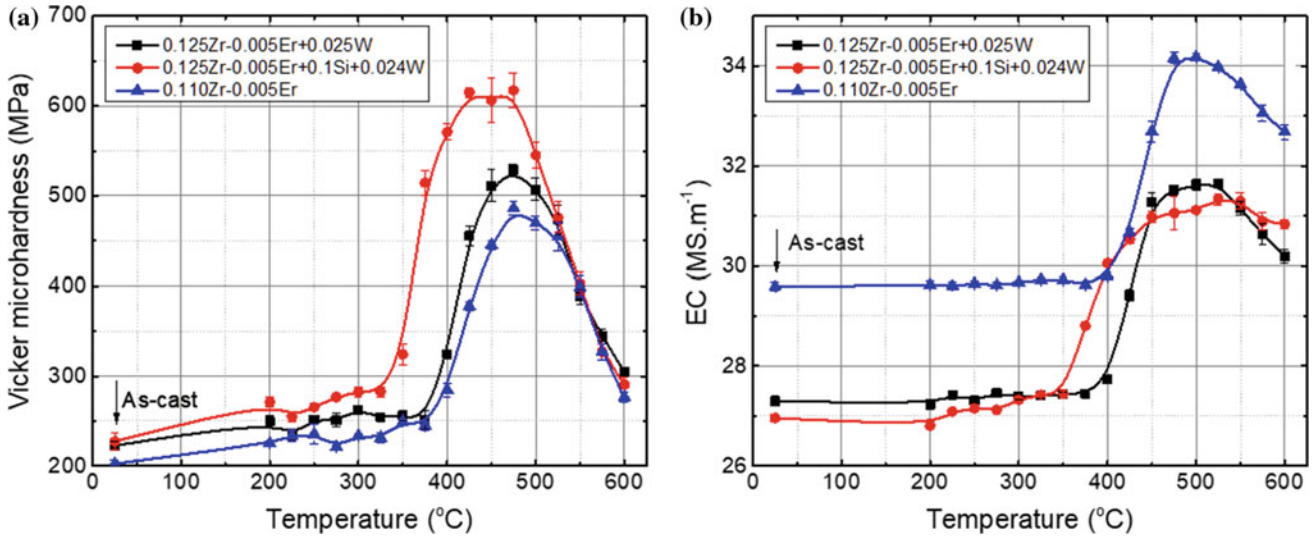

Fig. 2 **a** Vickers microhardness and **b** electrical conductivity evolution of the alloys during 3 h steps isochronal aging from 200 to 600 °C

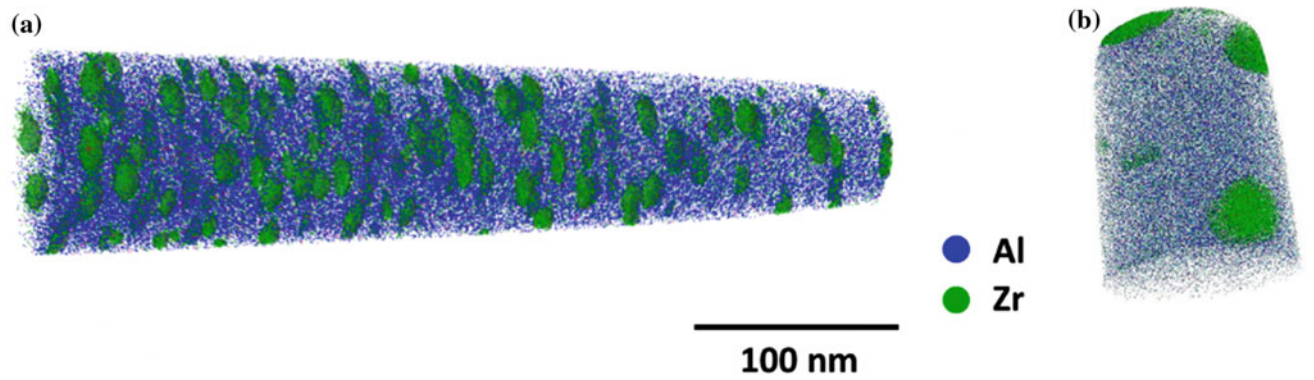

Fig. 3 APT reconstruction of the 0.125Zr-0.005Er-0.1Si-0.024 W alloy, isochronal aging from 200 °C to **a** 475 °C and **b** 525 °C, showing the $L1_2$ nanoprecipitates. Only Zr (in green) and Al (in blue) atoms are displayed

peak-aged sample with a mean precipitate radius of <R> = 2.1 ± 0.4 nm. Figure 4 displays the proximity histograms measured using the datasets in Fig. 3. In the peak-aged condition at 475 °C (Fig. 4a), precipitates exhibit an Er-rich core (radius of ~1 nm) similar to the $L1_2$ precipitates in the Al-Sc-Zr-Er system [18]. Total Er concentration of the precipitates, however, is ~0.2 at.% which is significantly lower than that reported for the Sc-containing Al_3(Sc,Zr,Er) nanoprecipitates (1–2 at.%) [13, 18]. This is attributed to the higher Zr level (0.11–0.12 at.%) of these alloys which does not permit homogenization of the as-cast structure, so that Er maintains its as-cast segregated distribution.

APT measurements (Fig. 4a) shows that in the peak-aged sample, W partitions significantly (~0.2 at.%) to the nanoprecipitates with a partitioning coefficient of $k_w^{L1_2/\alpha-Al} = C_w^{L1_2}/C_w^{\alpha-Al} \sim 7$. W concentration is higher at the Zr-rich shell, suggesting that W is diffusing into the precipitates. In the over-aged condition at 525 °C (Fig. 4b), larger nanoprecipitates (<R> = 5 nm) exhibit a higher amount of W (~0.4 at.%) which is almost uniformly distributed within the nanoprecipitates, indicating that more W atoms are incorporated into the $L1_2$ phase, progressively due to the enhanced diffusion of W at 525 °C. Total Er concentration of the nanoprecipitates increases to ~0.45 at.% at 525 °C. Higher Er concentration at the precipitate/matrix interface is also noteworthy which may be due to the diffusion of Er from the smaller precipitates dissolving into the matrix to the larger ones during the coarsening process (via evaporation-condensation mechanism).

Despite the substantial partitioning of W to the nanoprecipitates in this alloy system, no significant delay in the overaging of the W-modified alloys was observed during isochronal aging from 200 to 600 °C (Fig. 2). This unanticipated behavior can be explained by extremely sluggish diffusion of W in Al, which leads to the presence of an amount of W in the nanoprecipitates (~0.2 at.% at the peak

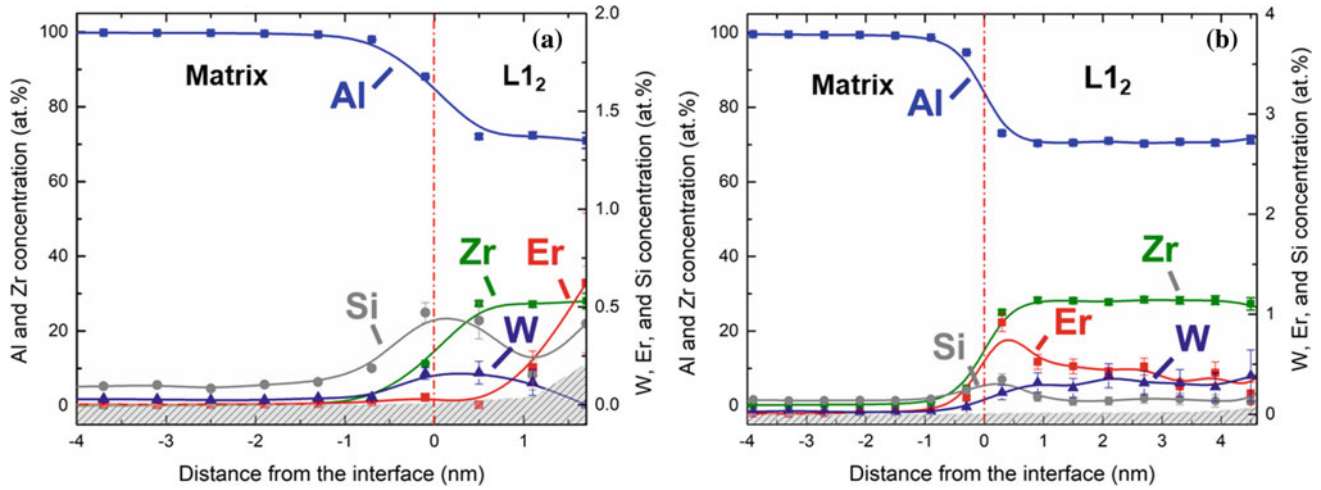

Fig. 4 Proximity histograms showing elemental distributions in the $L1_2$ nanoprecipitates of 0.125Zr-0.005Er-0.1Si-0.024 W, isochronally (3 h steps) aged from 200 °C to **a** 475 °C. **b** 525 °C, illustrating the significant partitioning of W to the L_{12} phase. The gray shaded areas represent the detection limit defined as one atom per proxigram bin (in at.%). The matrix/L_{12} interface (vertical dot-dash line) is defined as the inflection point of the Al concentration profile. The error bars represent the one-sigma statistical error [25]. Some error bars are smaller than the marker size

hardness) too low to affect coarsening; W diffusion becomes significant only at high temperatures when the precipitates are already coarse and have lost their strengthening effect. Silicon seems to have no significant effect on the diffusivity of W, however, it stimulates nucleation and growth of the nanoprecipitates leading to a high number density (5×10^{22} m^{-3}) in the peak-aged conditions.

Conclusions

The effect of W micro-additions (0.025 at.%) on the microstructure and mechanical properties of an Al-Zr-Er alloy, with and without Si, was investigated employing microhardness, electrical conductivity, optical microscopy and APT experiments. The following conclusions are deduced:

1. W partitions significantly to the $L1_2$ nanoprecipitates upon isochronal aging. APT measurements revealed ~0.2 at.% W within the nanoprecipitates in the peak-aged condition (475 °C) which increases to ~0.4 at.% at 525 °C (partitioning coefficients of ~7 and ~14, respectively).
2. Despite the strong partitioning of W to the nanoprecipitates, no significant effect was observed on the coarsening resistance of the nanoprecipitates. This unexpected behavior is explained by the extremely small diffusivity of W in Al, even in the presence of Si.
3. Microaddtions (0.1 at.%) of silicon leads to a higher peak microhardness (617 ± 19 MPa) compared to the alloys without Si (486 ± 7 and 528 ± 7 MPa for the W-free and W-modified alloys, respectively) due to the formation of a high number density of the nanoprecipitates (5×10^{22} m^{-3}) in the presence of Si.

Acknowledgements Atom-probe tomography was performed at the Northwestern University Center for Atom-Probe Tomography (NUCAPT). The LEAP tomograph at NUCAPT was purchased and upgraded with grants from the NSF-MRI (DMR-0420532) and ONR-DURIP (N00014-0400798, N00014-0610539, N00014-0910781, N00014-1712870) programs. NUCAPT received support from the MRSEC program (NSF DMR-1720139) at the Materials Research Center, the SHyNE Resource (NSF ECCS-1542205), and the Initiative for Sustainability and Energy (ISEN) at Northwestern University.

References

1. K.E. Knipling, R.A. Karnesky, C.P. Lee, D.C. Dunand, D.N. Seidman, Precipitation evolution in Al-0.1Sc, Al-0.1Zr and Al-0.1Sc-0.1Zr (at.%) alloys during isochronal aging, Acta Materialia 58(15) (2010) 5184–5195.
2. D.N. Seidman, E.A. Marquis, D.C. Dunand, Precipitation strengthening at ambient and elevated temperatures of heat-treatable Al (Sc) alloys, Acta Materialia 50(16) (2002) 4021–4035.
3. C. Booth-Morrison, D.C. Dunand, D.N. Seidman, Coarsening resistance at 400 C of precipitation-strengthened Al–Zr–Sc–Er alloys, Acta Materialia 59(18) (2011) 7029–7042.
4. K.E. Knipling, D.N. Seidman, D.C. Dunand, Ambient-and high-temperature mechanical properties of isochronally aged Al–0.06 Sc, Al–0.06 Zr and Al–0.06 Sc–0.06 Zr (at.%) alloys, Acta Materialia 59(3) (2011) 943–954.
5. C.B. Fuller, J.L. Murray, D.N. Seidman, Temporal evolution of the nanostructure of Al (Sc, Zr) alloys: Part I–Chemical compositions of Al3 (Sc1−xZrx) precipitates, Acta materialia 53(20) (2005) 5401–5413.

6. C.B. Fuller, D.N. Seidman, D.C. Dunand, Mechanical properties of Al (Sc, Zr) alloys at ambient and elevated temperatures, Acta Materialia 51(16) (2003) 4803–4814.
7. E. Marquis, D. Seidman, Nanoscale structural evolution of Al3Sc precipitates in Al (Sc) alloys, Acta materialia 49(11) (2001) 1909–1919.
8. M.E. Krug, D.C. Dunand, D.N. Seidman, Effects of Li additions on precipitation-strengthened Al-Sc and Al-Sc-Yb alloys, Acta Materialia 59(4) (2011) 1700–1715.
9. M. Van Dalen, T. Gyger, D. Dunand, D. Seidman, Effects of Zr on the Microstructure and Mechanical Properties of Al-Sc-Yb Alloys, Microscopy and Microanalysis 13(S02) (2007) 1618.
10. N. Vo, D. Dunand, D. Seidman, Improving aging and creep resistance in a dilute Al–Sc alloy by microalloying with Si, Zr and Er, Acta Materialia 63 (2014) 73–85.
11. M. Krug, D. Dunand, D. Seidman, Effects of Li additions on precipitation-strengthened Al–Sc and Al–Sc–Yb alloys, Acta Materialia 59(4) (2011) 1700–1715.
12. R.A. Karnesky, D.C. Dunand, D.N. Seidman, Evolution of nanoscale precipitates in Al microalloyed with Sc and Er, Acta Materialia 57(14) (2009) 4022–4031.
13. D. Erdeniz, W. Nasim, J. Malik, A.R. Yost, S. Park, A. De Luca, N.Q. Vo, I. Karaman, B. Mansoor, D.N. Seidman, Effect of vanadium micro-alloying on the microstructural evolution and creep behavior of Al-Er-Sc-Zr-Si alloys, Acta Materialia 124 (2017) 501–512.
14. M.E. Krug, A. Werber, D.C. Dunand, D.N. Seidman, Core–shell nanoscale precipitates in Al–0.06 at.% Sc microalloyed with Tb, Ho, Tm or Lu, Acta Materialia 58(1) (2010) 134–145.
15. C. Booth-Morrison, D.N. Seidman, D.C. Dunand, Effect of Er additions on ambient and high-temperature strength of precipitation-strengthened Al–Zr–Sc–Si alloys, Acta Materialia 60(8) (2012) 3643–3654.
16. M.E. Van Dalen, T. Gyger, D.C. Dunand, D.N. Seidman, Effects of Yb and Zr microalloying additions on the microstructure and mechanical properties of dilute Al–Sc alloys, Acta Materialia 59 (20) (2011) 7615–7626.
17. A. De Luca, D.C. Dunand, D.N. Seidman, Mechanical properties and optimization of the aging of a dilute Al-Sc-Er-Zr-Si alloy with a high Zr/Sc ratio, Acta Materialia 119 (2016) 35–42.
18. A. De Luca, D.C. Dunand, D.N. Seidman, Microstructure and mechanical properties of a precipitation-strengthened Al-Zr-Sc-Er-Si alloy with a very small Sc content, Acta Materialia 144 (2018) 80–91.
19. S. Wen, K. Gao, Y. Li, H. Huang, Z. Nie, Synergetic effect of Er and Zr on the precipitation hardening of Al–Er–Zr alloy, Scripta materialia 65(7) (2011) 592–595.
20. H. Li, J. Bin, J. Liu, Z. Gao, X. Lu, Precipitation evolution and coarsening resistance at 400 C of Al microalloyed with Zr and Er, Scripta Materialia 67(1) (2012) 73–76.
21. S. Wen, K. Gao, H. Huang, W. Wang, Z. Nie, Precipitation evolution in Al–Er–Zr alloys during aging at elevated temperature, Journal of Alloys and Compounds 574 (2013) 92–97.
22. N.Q. Vo, D.N. Seidman, D.C. Dunand (2016) Aluminum superalloys for use in high temperature applications, US. Patent 9.453,272 B2, Sep. 27 2016.
23. K.E. Knipling, D.C. Dunand, D.N. Seidman, Criteria for developing castable, creep-resistant aluminum-based alloys - A review, Zeitschrift Fur Metallkunde 97(3) (2006) 246–265.
24. L.F. Mondolfo, Aluminum alloys: structure and properties, Elsevier 2013.
25. O.C. Hellman, J.A. Vandenbroucke, J. Rüsing, D. Isheim, D.N. Seidman, Analysis of three-dimensional atom-probe data by the proximity histogram, Microsc. Microanal. 6(5) (2000) 437–444.
26. C. Booth-Morrison, Z. Mao, M. Diaz, D.C. Dunand, C. Wolverton, D.N. Seidman, Role of silicon in accelerating the nucleation of Al-3(Sc,Zr) precipitates in dilute Al-Sc-Zr alloys, Acta Materialia 60(12) (2012) 4740–4752.